A SOLAR REFLECTANCE METHOD FOR RETRIEVING THE OPTICAL THICKNESS AND DROPLET SIZE OF LIQUID WATER CLOUDS OVER SNOW AND ICE SURFACES

S. Platnick[1,2], J. Y. Li[2,3], M. D. King[2], H. Gerber[4], P. V. Hobbs[5]

[1]University of Maryland Baltimore County, Baltimore, MD
[2]NASA Goddard Space Flight Center, Greenbelt, MD
[3]SM&A Corporation, Vienna, VA, [4]Gerber Scientific Inc., Reston, VA
[5]University of Washington, Seattle, WA

Submitted to:
Journal of Geophysical Research – Atmospheres
FIRE-ACE Special Issue
15 December 1999

revised: 11 May 2000

Corresponding author address:

S. Platnick
Code 913
NASA GSFC
Greenbelt, MD 20771
platnick@climate.gsfc.nasa.gov

Abstract

Cloud optical thickness and droplet effective radius retrievals from solar reflectance measurements are traditionally implemented using a combination of spectral channels that are absorbing and non-absorbing for water particles. Reflectances in non-absorbing channels (e.g., 0.67, 0.86, 1.2 μm spectral window bands) are largely dependent on cloud optical thickness, while longer wavelength absorbing channels (1.6, 2.1, and 3.7 μm window bands) provide cloud particle size information. Cloud retrievals over ice and snow surfaces present serious difficulties. At the shorter wavelengths, ice is bright and highly variable, both characteristics acting to significantly increase cloud retrieval uncertainty. In contrast, reflectances at the longer wavelengths are relatively small and may be comparable to that of dark open water.

A modification to the traditional cloud retrieval technique is presented. The new algorithm uses only a combination of absorbing spectral channels for which the snow/ice albedo is relatively small. Using this approach, retrievals have been made with the MODIS Airborne Simulator (MAS) imager flown aboard the high altitude NASA ER-2 from May-June 1998 during the Arctic FIRE-ACE field deployment. Data from several coordinated ER-2 and *in situ* University of Washington Conviar-580 aircraft observations of liquid water stratus clouds are examined. MAS retrievals of optical thickness, droplet effective radius, and liquid water path are shown to be in good agreement with *in situ* measurements. The initial success of the technique has implications for future operational satellite cloud retrieval algorithms in polar and wintertime regions.

1. Introduction

The First ISCCP (International Satellite Cloud Climatology Project) Regional Experiment – Arctic Clouds Experiment (FIRE-ACE) was conducted in the vicinity of Barrow, Alaska and northward over the Chukchi and Beaufort Seas. The overall goal was to better understand cloud-surface interactions and radiative effects in the Arctic Ocean region [see *Curry et al.*, 2000 for review]. Of specific interest to the FIRE project was development and validation of satellite and aircraft remote sensing techniques for retrieving cloud properties. In particular, retrievals of both cloud optical thickness and particle size are necessary in understanding and parameterizing cloud radiative effects in shortwave and longwave spectral regions [*Slingo*, 1990; review of *Wielicki et al.*, 1995]. Cloud particle size retrievals are also important in studies of the so-called indirect effect of aerosols on climate, and in determining susceptibility to microphysical modification of cloud albedo [*Twomey*, 1974; *Charlson et al.*, 1987; *Twomey*, 1991] and precipitation processes [*Albrecht*, 1989; *Pincus and Baker*, 1994; *Austin et al.*, 1995]. In radiative studies, it is the *effective radius* ($r_e = \overline{r^3} / \overline{r^2}$) that is the important measure of the particle size distribution. Retrievals of both cloud parameters are especially problematic using solar reflectance techniques in the presence of highly reflective surfaces such as snow and sea ice in polar regions. The FIRE-ACE time period overlapped with the Surface Heat Budget of the Arctic Ocean (SHEBA) project, which included an icebreaker ship frozen in the pack ice. The ice station, located about 700 km northwest of Barrow during the experiment, included a number of remote sensing and meteorological instruments useful for validating cloud retrievals.

Previous algorithms for retrieving cloud optical thickness and effective particle radius from reflectance measurements have used spectral bands that are both absorbing and nonabsorbing for water particles. In particular, these are generally bidirectional reflectance measurements, i.e., a function of both solar and viewing angles (as opposed to flux reflectance or albedo measurements). Reflectances in nonabsorbing channels (e.g., 0.67, 0.86, 1.2 μm spectral window bands) are largely dependent on cloud optical thickness. Only a relatively small decrease in reflectance occurs with increasing particle size due to a corresponding slight increase in the particle forward scattering (characterized by the scattering asymmetry parameter). However, reflectances at longer wavelengths (1.6, 2.1, and 3.7 μm window bands, collectively referred to as *near-infrared* in this paper) are extremely sensitive to cloud particle absorption. The single scattering

albedo (difference between unity and fractional particle absorption) decreases in the 2.1 μm band from about 0.99 to 0.96 as effective radius increases from 5 to 20 μm. Since particle absorption is proportional to size, this sensitivity to single scattering albedo provides information on cloud particle size. Such a combination of absorbing and non-absorbing reflectance measurements is advantageous in that it allows for a nearly orthogonal separation of optical thickness and particle size in the measurements, especially for thicker clouds (see section 2).

In principle, this technique is useful for ice particles as well as liquid water droplets. However, ice clouds will, in general, present an additional retrieval unknown – particle habit. Liquid water cloud retrievals, along with validation case studies, have been described by *Twomey and Cocks* [1982; 1989], *Foot* [1988], *Nakajima and King* [1990], *Nakajima et al.* [1991], and *Platnick and Valero* [1995]. Ice cloud retrieval validation studies [e.g., *Ou et al.*, 1995; *Young et al.*, 1998; Rolland et al., 2000] have also been discussed. In the present study, we deal exclusively with liquid water cloud retrievals using solar reflectance measurements. Since section 2 of this paper will discuss only basic retrieval principles, the reader is referred to the cited studies for further detail.

The use of a visible or other useful nonabsorbing band presents serious difficulties for cloud retrievals over ice and snow surfaces. At these shorter solar wavelengths, snow/ice can be both bright and highly variable, each acting to significantly increase the uncertainty in retrieving cloud parameters. Retrieval algorithms are inherently more sensitive over dark surfaces where the cloud-surface contrast is greatest. Bright surfaces (e.g., an ice albedo of 0.5 in the visible) acts to reduce, or mask, the effect of the cloud on the overall measured reflectance. This is especially problematic for thin clouds having a reflectance of the same order as the surface reflectance variability. Of course, accurate knowledge of a large surface reflectance is essential regardless of cloud thickness. In contrast, snow/ice reflectances at the longer wavelengths are relatively small and may be comparable to that of dark open water.

A modification to the traditional cloud retrieval technique is described in this paper. The new algorithm uses only a combination of absorbing spectral channels for which the snow/ice albedo is relatively small. Specifically, the 1.6 μm band reflectance is used essentially as a surrogate for the traditional nonabsorbing band, in conjunction with a more absorbing 2.1 or 3.7 μm band. This approach significantly reduces (or practically eliminates in the case studies that follow) the effect of the snow/ice surface. However, the reduced surface effect comes at the expense of the relative orthogonality between the two

measurements and the optical thickness and effective radius retrievals. Using this method, liquid water cloud retrievals have been made with the MODIS Airborne Simulator (MAS) imager flown aboard NASA's high altitude ER-2 aircraft during the FIRE-ACE field deployment. While the FIRE-ACE observation period extended from April to July 1998, ER-2 operations were conducted between May 18 and June 6 out of Fairbanks, Alaska.

The MAS is a 50 channel scanning spectrometer that provides spectral coverage from the visible through the infrared via four separate grating assemblies. The particular MAS spectral channels useful for the cloud studies of this paper were centered at 0.66, 0.87, 1.62, 2.13, 3.75, and 10.71 μm; the channel bandpasses varied from about 45 nm in the visible and near-infrared, to 140nm at 3.75 μm and 540 nm in the thermal infrared. Onboard blackbodies are used for calibration of the thermal emissive channels (including the 3.7 μm channel). A laboratory integrating sphere is used for calibration of channels in the solar spectrum (up to 2.4 μm). Spectral laboratory calibrations are also routinely made. At nominal ER-2 altitudes (20 km), the nadir spatial resolution is 50 m at the surface corresponding to a cross-track swath width of about 37 km (716 pixels). Further details are given by *King et al.* [1996]. Cloud retrieval validation studies using this instrument have been reported by *Platnick et al.* [2000] for California marine stratus clouds.

In this paper, data from coordinated ER-2 and University of Washington Convair-580 aircraft observations of liquid water stratus clouds are examined. Size retrievals are compared with *in situ* cloud profile measurements of droplet effective radius made with the Particle Measuring Systems FSSP-100 probe. Optical thickness and liquid water path retrievals are compared with values derived from the Gerber Scientific, Inc. cloud integrating nephelometer (also known as the "*g*-meter") and PVM-100A [*Gerber et al.*, 1994, 2000], respectively. Section 2 discusses the difficulties of retrievals over bright surfaces and the tradeoffs in using only those spectral bands with significant water absorption. Section 3 summarizes sea ice and snow reflectance measurement in the Arctic obtained during previous field campaigns. In section 4 we discuss two liquid water cloud case studies, including a low-level boundary layer cloud and an extensive, but spatially variable, supercooled mid-level stratus deck. For both cases, MAS retrievals are shown to be in good agreement with *in situ* measurements.

2. Cloud Retrievals over Bright Surfaces

As discussed above, simultaneous bidirectional reflectance measurements in visible and near-infrared bands have been routinely used to infer cloud optical thickness (τ_c) and droplet effective radius (r_e) of liquid water clouds. Retrievals are based on comparisons between measured reflectances and those calculated for plane-parallel homogeneous clouds. That is, retrievals give the optical thickness and effective radius of a plane-parallel homogeneous cloud having reflectances best matching the measurements for the given set of angles.

The bidirectional reflectance in a visible or nonabsorbing band has the functional dependence $R_{VIS} \approx R_{VIS}(\tau_c)$, that is, optical thickness can be largely determined from this single measurement (the functional dependence on solar and viewing geometry is understood). In the useful water-absorbing near-infrared bands, located in the 1.6, 2.1, or 3.7 μm spectral region, reflectance can be a significant function of both quantities (i.e., $R_{NIR} = R_{NIR}(\tau_c, r_e)$) although for large absorption and/or cloud optical thickness, $R_{NIR} \approx R_{NIR}(r_e)$. Since these bands are located in atmospheric windows to minimize the effect of molecular absorption, further mention of absorption will be understood to refer to water droplets and not water vapor or other gases. Droplet size information can be inferred only from these absorbing bands. In principle, simultaneous reflectance measurements using a combination of any two bands (providing *at least* one has significant absorption) will allow for the solution of the two unknowns. For example, a combination of a 1.6 and 2.1 μm band reflectance measurement could be used instead of the traditional nonabsorbing and absorbing band combination. However, only the latter combination allows for near-othogonality between the two solutions. These concepts are discussed below.

Consider a cloud retrieval obtained from simultaneous visible and 2.1 μm band reflectance measurements for the ideal situation where the cloud overlies a surface having a small albedo in both bands. A useful means for understanding the information content of the two reflectance measurements is to transform the retrieval solution space (contours of constant optical thickness and effective radius) into the reflectance space [*Nakajima and King*, 1990; *Rawlins and Foot*, 1990]. An example is shown in the plots of Fig. 1a for the two corresponding MAS bands and the plane-parallel geometry given in the caption. The surface albedo for each, representative of open water, is indicated on the figure. With such a plot, the cloud retrieval problem reduces to the solution consistent with the point specified by reflectance measurement in the two spectral bands. Note that

solution contours are nearly orthogonal over much of the measurement space, especially at the larger optical thicknesses. For exact orthogonality, an error in the reflectance measurement from one spectral band (caused by either instrument calibration or modeling errors) does not affect the solution obtained with the other band. Though multiple solutions are seen for the 2 µm effective radius contour, such a size has been found to be unrealistic for real clouds.

Now consider a cloud overlying sea ice or snow. Figure 1b demonstrates the difficulties in retrieving cloud optical thickness using a spectral band for which the surface is both bright and variable. The retrieval solution space is shown for the same spectral bands of Fig. 1a, but with a Lambertian surface reflectance of 0.50 in the visible; the surface albedo in the 2.1 µm band is assumed unchanged for an ice surface. The plausibility of these reflectances for ice and snow surfaces is discussed in section 3. Two sources for increased error sensitivity in the optical thickness contours are evident. First, the optical thickness contours have been moved to the right along the abscissa, narrowing their spacing. Because of this contour compression, optical thickness retrievals are more sensitive to visible reflectance measurement error than for the situation of Fig. 1a. This error magnification is inherent to retrievals over bright surfaces. The physical cause is the relatively smaller reflectance increase contributed by the cloud (even a semi-infinite cloud would not be detected with a non-absorbing band in the extreme case of unity surface albedo). Second, an uncertainty in the underlying sea ice albedo for the visible band results in an uncertainty in the horizontal position of the left side thickness contours (i.e., reflectance for ice plus thin cloud is highly uncertain) causing a potentially large retrieval uncertainty. As an example of this second error sensitivity, inspection of Figs. 1a,b suggest that retrieval of optical thickness to within ±20% for a nominal cloud with $\tau_c = 10$ and $r_e = 10$ µm, would require knowing the surface reflectance to better than about 10% relative (i.e., 0.50 ± 0.05). As discussed in the next section, sea ice and snow albedo can be highly variable with a significant seasonal variability. It is unrealistic to expect that the spectral surface albedo of these surfaces can be known to the desired accuracy, both temporally and spatially, for useful operational satellite cloud retrievals [*Wielicki et al.*, 1995]. Existence of broken sea ice, common near Barrow during FIRE-ACE, exacerbates the difficulty in specifying the effective area-averaged surface albedo needed for cloud retrievals.

An approximation for the increased error sensitivity in the optical thickness retrieval from both these effects can be found from two-stream formulae for flux reflectance with conservative scattering. The combined cloud-surface reflectance is given

by $R_m = R_c + R_s(1-R_c)^2/(1-R_sR_c)$ where R_m is the total *measured* reflectance in the nonabsorbing band, R_s is the surface reflectance, and R_c is the reflectance of the cloud being observed when overlying a black surface; the term in the denominator accounts for multiple reflections between the cloud and surface. Isolating the cloud reflectance terms gives $R_c = (R_m - R_s)/[1-R_s(2-R_m)]$. Substitution of a two-stream reflectance formula having the general form $R_c = \gamma\tau_c/(1+\gamma\tau_c)$, where τ_c is the cloud optical thickness and $\gamma$is a constant depending on the droplet scattering asymmetry, gives

$$\tau_c = \frac{1}{\gamma}\,\frac{R_m - R_s}{(1-R_m)(1-R_s)}\,. \qquad (1)$$

The asymmetry parameter, g, indicates the amount of forward scattering which increases with droplet size. For example, $g \approx 0.84\text{-}0.87$ corresponding to $r_e = 5\text{-}15\,\mu m$ in the visible. Using $\gamma = (1-g)/2$ (*Bohren* [1987]), $\gamma^{-1} = 12.5\text{-}15.4$ over the same size range. The above formula is a simple approximation for the *retrieved* optical thickness corresponding to some measured reflectance and a presumed surface reflectance. The small effect of droplet size on the retrieval (non-vertical contour lines in Fig. 1b) via the asymmetry parameter, i.e., γ, will be neglected until the numerical calculations at the end of this section.

Assuming the surface reflectance is specified without error, the relative uncertainty in the optical thickness retrieval due to measurement uncertainty (e.g., instrument calibration) is given by derivative $\partial \ln\tau_c/\partial R_m$. This corresponds to the first source of retrieval error sensitivity discussed earlier. Retrieval uncertainty due to uncertainty in model calculations of the visible band reflectance is also covered by this derivative. It can be shown that the derivative is given by

$$\frac{\partial \ln\tau_c}{\partial R_m} = \frac{1}{\gamma\,\tau_c}\,\frac{1}{(1-R_m)^2}\,. \qquad (2)$$

Likewise, because of symmetry between R_m and R_s in Eq. 1, the sensitivity to uncertainty in knowledge of the surface reflectance, assuming no measurement error, is

$$\frac{\partial \ln \tau_c}{\partial R_s} = \frac{-1}{\gamma \tau_c} \frac{1}{(1-R_s)^2} . \quad (3)$$

As an example, consider a cloud with $\tau_c = 10$, $g = 0.85$, $\gamma = (1\text{-}g)/2 = 0.075$, and a surface reflectance of $R_s = 0.50$, giving a cloud reflectance of $R_c = 0.43$ and a total measured reflectance of $R_m = 0.64$ (similar to FIRE-ACE cloud retrievals discussed in section 4). Then Eq. 3 implies that an increase in R_s of 0.05 would result in a decrease in the retrieved cloud optical thickness by over 25%. Or alternatively, if the retrieval is made with an assumption that $R_s = 0.50$ but the actual value is $R_s = 0.55$, then the relative error in the retrieved optical thickness is $\Delta\tau_c/\tau_c \approx +30\%$. Similarly, Eq. 2 gives a retrieval error of $\Delta\tau_c/\tau_c \approx +50\%$ if the measured reflectance R_m is in error by an amount of +0.05. In contrast, for the identical cloud over a dark surface with the assumption $R_s = 0.05$, resulting errors due to the same underestimation in the surface reflectance and overestimation in the measured reflectance are reduced to $\Delta\tau_c/\tau_c \approx +7\%$ and +22%, respectively. In summary, for this rather typical cloud example, optical thickness retrieval uncertainty due to a realistic uncertainty in the knowledge of the underlying sea ice surface reflectance, is greater by about a factor of four than retrieval uncertainty caused by a similar absolute uncertainty in the reflectance of a dark surface. Retrieval uncertainty due to measurement error is increased by a factor of two when the ice surface is present.

As discussed, the use of a non-absorbing band is not inherent to the retrievals, and two absorbing bands can also be used. The snow/ice surface albedo can be very small in all near-infrared bands as shown in the next section. Accordingly, Fig. 2a shows the solution space when the visible channel is replaced by a 1.6μm channel (absorbing for cloud droplets but much less than for the 2.1 μm band). The surface albedo in these near-infrared bands is assumed equivalent to that of open water. With droplet absorption, two stream formulae become difficult to manipulate analytically and so approximations for error sensitivity are no longer feasible for this situation. But such a retrieval would clearly have little dependence on sea ice characteristics, or fractional ice coverage. The disadvantage is that the solutions no longer have an orthogonal region, and so measurement error in one channel will *always* cause error in the retrieval of both cloud parameters. Specifically, retrieval error in one parameter causes a proportional (same sign) error in the other. An increased sensitivity to measurement error, compared to the traditional non-absorbing band method with a dark surface, is also evident. Figure 2b

shows the improved situation obtained with use of a 3.7 μm band. However, cloud thermal emission in this band (also dependent on optical thickness and effective radius) can be a significant part of the measured upwelling radiance, thereby complicating the retrieval [*Arking and Childs*, 1985; *Han et al.*, 1994; *Platnick and Twomey*, 1994].

Retrieval sensitivity to measured reflectances were determined numerically for the band combinations and surface reflectances of Figs. 1,2. Sensitivities are given in Table 1 (same geometry as Figs. 1,2, and $\tau_c = 10$, $r_e = 10\,\mu m$). The calculations are approximately valid for small changes in the surface reflectance as well. First consider sensitivities to the less absorbing band reflectance, R_1, given in the table. For the 1.6 and 2.1μm band retrieval combination (Fig. 2a), a +10% increase in the 1.6 μm reflectance (i.e., $\partial \ln R_1 = +0.10$ in the table) results in a +38% change in the retrieved cloud optical thickness and a +12% increase in the retrieved effective radius. These are smaller than comparable sensitivities for the 0.67, 2.1 μm band combination with a visible surface albedo of 0.50 (Fig. 1b); now a +10% increase in the visible reflectance gives a +58% and +19% change in the retrieved optical thickness and effective radius, respectively. In contrast, sensitivities to $\partial \ln R_2$ are larger for the 1.6, 2.1 μm combination. Note that retrieval sensitivity is always smaller when using the 3.7 μm band (any combination) due to the near orthogonality of the solution space. Sensitivities corresponding to Fig. 1a are smaller overall as expected. Viewing angle dependencies exist but the above conclusions remain the same. Retrieval error sensitivity tends to increase with solar and viewing zenith angle for all band combinations, most notably for optical thickness. However in some instances, effective radius retrieval sensitivity decreases slightly at the more oblique angles.

3. Spectral Albedo Measurements of Arctic Sea Ice and Snow

The utility of near-infrared water absorbing bands for cloud retrievals over snow/ice surfaces requires a small, hopefully insignificant, albedo in this spectral region compared with shorter wavelengths. Ground-based snow/ice spectral surface albedo and bidirectional reflectance measurements have been reported for a variety of Arctic locations and seasons [*Grenfell and Perovich*, 1984; *Perovich*, 1994; *DeAbreu et al.*, 1995; *Curry et al.*, 2000; *Arnold et al.*, 2000]. The studies show that the albedo of sea ice is highly dependent on the presence of air bubbles and brine. Overlying snow greater than several centimeters in thickness dominates the overall reflectance, which becomes largely dependent on snow grain size. The onset of surface melting results in dramatic decreases

in reflectance. The current interest is in large area-averaged measurements of albedo of springtime Arctic sea ice in the particular visible and near-infrared spectral bands used for cloud retrievals. Such data are mostly available from the Cloud Absorption Radiometer (CAR) flown aboard University of Washington aircraft during previous Arctic field campaigns and also in FIRE-ACE.

3.1 CAR measurements

The CAR is a narrowband visible/near-infrared scanning radiometer mounted in the nose cone of the University of Washington Convair-580 aircraft (previously on the University of Washington C-131A). Spectral channels include the 0.68, 0.87, 1.2, 1.6, and 2.1 μm bands; the 3.7 μm band is not covered. Though originally designed for use in thick cloud layers, the instrument's unique 190º zenith-to-nadir scanning capability also allows it to be used to map surface hemispheric upwelling bidirectional radiance fields. Such measurements are obtained as the aircraft flies repeated circles (approximately 3 km in diameter) over a study site, at a typical altitude of 0.5-1.0 km. Aircraft roll during the circular flight tracks is compensated for by rotating the CAR assembly within the nose cone. Surface albedo is derived from integration over the CAR upward hemispheric radiance measurements in conjunction with solar spectral flux tables. The derived albedo is effectively averaged over a spatial scale on the order of 3 km (95% of the reflected energy is captured within this scale for isotropic reflectance). Further details of the instrument and bidirectional reflectance measurements derived from this sensor can be found in *King et al*. [1986], *Tsay et al.* [1998], *Soulen et al.* [2000], and *Arnold et al.* [2000].

CAR bidirectional measurements were made during two previous Arctic field deployments: the Arctic Lead Experiment (LEADEX) during April 1992 and the June 1995 Arctic Radiation Measurements in Column Atmosphere-Surface System (ARMCAS). Both experiments were conducted in the vicinity of Prudhoe Bay, Alaska and over the Beaufort and Chukchi seas. A complete analysis of the reflectance data for melt-season sea ice, snow/ice over the tundra, and clear tundra is discussed by *Arnold et al.* [2000]. While such measurements can be made under diffuse conditions when higher cloud bases are present (more appropriate to the cloud retrieval problem), the analyzed data from these experiments were taken under clear sky conditions. Solar zenith angles in this region varied from about 65º to 50º between April and June during CAR acquisition times. A summary of the CAR albedo calculations for sea ice and snow/ice over tundra

are given in Fig. 3. Albedo for the shorter wavelengths is seen to be large and variable, both being problematic for cloud retrievals (Fig. 1a; Eqs. 2, 3). In contrast, albedo in the 1.6 and 2.1 µm bands during June is only a few percent, similar to open water, and with relatively small variability. However, 1.6 µm snow and ice albedos in April are significantly larger than in June, though still much smaller than at shorter wavelengths (2.1 µm data not available). Figure 3 albedo calculations do not include an atmospheric correction appropriate to the aircraft altitude. However, it is exactly this combined surface-atmosphere albedo near cloud base that is relevant to the cloud retrieval problem.

The observed decrease in spectral sea ice albedo between April and June for the two previous field campaigns were also found in solar broadband albedo aircraft measurements during FIRE-ACE [reported by *Curry et al.*, 2000]. The CAR observations are also consistent with Arctic springtime ground observations of sea ice albedo under diffuse sky conditions [*Grenfell and Perovich*, 1984; *DeAbreu et al.*, 1995] where reflectance is reduced across the solar spectrum as overlying snow begins to melt. MAS bidirectional reflectance measurements of sea ice throughout the Barrow region during a clear sky ER-2 flight (May 29, 1998) are also shown in Fig. 3. These data points also confirm the extremely low reflectance for the near-infrared bands during this time of year. So at least during the late springtime period, near-infrared ice/snow albedo in this region is likely to be comparable to dark open water and therefore ideally suited for cloud retrievals.

3.2 MAS estimates for the 3.7 µm band

Surface characteristics relevant to the 3.7 µm band include emissivity as well as reflectance (coupled as described below). However, for retrieval purposes, the influence of the surface on 3.7 µm measurements is limited to clouds with optical thickness less than about 6 due to large droplet absorption in the band [*Platnick and Valero*, 1995]. The clouds described in section 4 are optically thicker than this amount, so knowledge of snow and ice properties in the band is not required. For thinner clouds, this would not have been the case.

Field measurements of 3.7 µm band snow/ice albedos have not been reported. However, laboratory measurements in this band were made by *Salisbury et al.* [1994] for a variety of conditions (snow grain size, dry and wet snow, granular crust). Their results indicate that 3.7 µm albedos are generally smaller than those for the 2.1 µm band, with values of just a few percent. This is not unexpected given the larger relative bulk ice

absorption in the 3.7 µm band [*Warren*, 1984], though relative differences in the effective particle scattering phase function might provide exceptions at some angles. This conclusion can be checked with MAS 3.7 µm channel measurements from clear sky snow/ice scenes. The reflected 3.7 µm radiance at the surface is $\mu_0 F_0 t(\mu_0) R_{sfc}(\mu_0,\mu)/\pi$, where F_0 is the solar flux in the band, R_{sfc} is the surface bidirectional reflectance, t is the transmittance from the top of the atmosphere to cloud top, and μ_0 and μ are the cosine of the solar and viewing zenith angles, respectively. The total radiance at the altitude of the ER-2 (nominal 20 km) is then $t(\mu)t(\mu_0)\mu_0 F_0 R_{sfc}(\mu_0,\mu)/\pi + t(\mu)\mathrm{B}(T_{sfc})\epsilon_{sfc}(\mu)$, where ϵ_{sfc} is the surface emissivity, and $\mathrm{B}(T_{sfc})$ is the Planck radiance for the surface skin temperature T_{sfc}. For any particular angular direction μ, the surface albedo is given by Kirchoff's law as $A_{sfc}(\mu) = 1 - \epsilon_{sfc}(\mu)$. Assuming $R_{sfc}(\mu_0,\mu) \approx A_{sfc}(\mu)$, the total band radiance is approximated as $t(\mu)t(\mu_0)\mu_0 F_0 A_{sfc}/\pi + t(\mu)\mathrm{B}(T_{sfc})(1 - A_{sfc})$. The accuracy of a MAS-derived estimate for surface albedo and emissivity depends on angular variations in the reflectance quantities, and knowledge of the atmospheric water vapor profile and surface temperature.

A clear sky scene in the vicinity of Barrow Alaska on May 29, 1998 is shown in Fig. 4a. (further described in section 4.1.1). Several sea ice and snow on tundra scenes were analyzed. Atmospheric transmittance in the 3.7 µm band, calculated using the correlated *k*-distribution method of *Kratz* [1995], is primarily dependent on water vapor which was determined from a SHEBA ice station rawinsonde launched at 2315 UTC on May 29. Surface skin temperature was assumed to be 273 K. The above approximation indicates a surface albedo less than 0.01. The result was not critically dependent on the water vapor profile. Larger surface temperatures further reduce the derived albedo until no solution was possible (i.e., albedo less than zero). Overall, 3.7 µm radiance measurements appear consistent with a surface albedo smaller than that of shorter wavelength near-infrared retrieval bands.

4. Liquid Water Cloud Retrievals from FIRE-ACE

Simultaneous cloud microphysical and optical thickness retrievals were performed on a variety of liquid water clouds imaged by the MAS during the FIRE-ACE ER-2 deployment period. Retrievals used the spectral technique described in section 2, with the 1.6 µm band used as a surrogate for a nonabsorbing band in conjunction with a 2.1 or 3.7 µm band (e.g., Figs. 2a,b, respectively). Otherwise, the algorithm is identical to *Platnick et al.* [2000]. Of the 11 ER-2 flights flown from May 18–June 6, coordinated

cloud *in situ* sampling by the University of Washington Convair-580 aircraft occurred during 6 of the flights. Two of these coordinations were in relatively uniform cloud regions useful for liquid water validation purposes. These two case studies are discussed next.

4.1 Low-level boundary layer stratus cloud on June 6, 1998

An extensive boundary layer stratus cloud was overlying the coastal region near Barrow at midday on June 6, 1998. The cloud was about 300 m thick with a cloud-top height and temperature of about 800 m and 268 K, respectively, as determined from *in situ* penetrations. The ER-2 takeoff from Fairbanks, Alaska was at 1855 UTC, with an objective to fly several flight legs over the Barrow region during the course of the day's flight. The Convair-580 takeoff from Barrow was at 1941 UTC, followed by *in situ* profile measurements during the subsequent ascent through the cloud layer. A second profile was made in this region at 2310 UTC. Such vertical transits through the cloud are required for determining integrated optical and liquid water paths. Also, an appropriate weighting can then be applied to the droplet effective radius profile for comparison with the vertically averaged reflectance-based retrievals [*Platnick*, 2000]. The coordination closest in time with the University of Washington Convair-580 *in situ* measurements occurred during the initial ER-2 overpass at 2002 UTC on the original northwest flight track out of Fairbanks. While this was 21 minutes after the first *in situ* profile, the later Convair-580 profile showed just a small change in droplet effective radius over the three-and-one-half hour gap (cloud-top sizes increased by about 1.3 μm). Further, the retrievals discussed later indicate relatively uniform effective radii throughout the region at the time of the first ER-2 overpass.

4.1.1 Clear sky observations of the retrieval region

Overflights of the North Slope of Alaska Atmospheric Radiation Measurement (NSA ARM) surface site near Barrow occurred at least once during each ER-2 flight, typically during the initial flight from Fairbanks out over the sea ice. This first pass over the ARM site generally occurred about the same time each day (2000 UTC) due to a common takeoff time. As such, clear-sky MAS images of this region were obtained twice in the week prior to the occurrence of the June 6 boundary layer cloud. These earlier images demonstrate the variable and often unpredictable nature of the land and ocean surface reflectances near the coast during this time of year. Figure 4a shows a geolocated

MAS visible image over the Barrow area on May 29, 1998. Sea ice is seen to be widespread across the northern end of the image, with open water near the coast and snow covering the tundra. Just four days later (Fig. 4b), the tundra had completely cleared of snow, although a myriad of melt-ponds remained frozen. Ice in the inlet southeast of Pt. Barrow had melted as well. Also, the offshore open water area appears to have diminished somewhat, with a substantial sea ice fraction towards the southwest. Clearly, knowledge of such fine scale detail in the surface characteristics on a day-to-day basis would be extremely challenging for useful cloud validation studies, much less global scale retrievals. At the time of the MAS cloud observations three days later, the coastal open water area appeared to have diminished further, as seen in CAR measurements taken beneath the stratus deck as the Convair-580 was flying parallel to and just offshore the coast. MAS bidirectional reflectance measurements of the wet, recently melted, tundra obtained from the June 2 image (Fig. 4b) were found to be about 0.30 ± 0.14, 0.06 ± 0.04, and 0.04 ± 0.03 in the 0.67, 1.6, and 2.1 µm bands, respectively. Observations were for a solar zenith angle of 54º and with near-nadir views. No atmospheric corrections were made, a situation more applicable to the cloud retrieval problem which requires reflectance referenced to the cloud-base altitude. The low near-infrared surface reflectances, similar to that of the ice and open water, suggest that little discontinuity should be seen across the ocean-land boundary in the retrievals.

4.1.2 Retrievals

Figure 5a shows the visible MAS image at the time of the cloud retrieval on June 6. The land-sea boundary is easily observed through the cloud. Frozen ponds are noted as well as the open water inlet southeast of Pt. Barrow. Conversely, because of the low albedo for all surfaces, the corresponding 1.6 µm band image (Fig. 5b) shows a uniform cloud across the coastal area. A sharp boundary between a substantially thinner cloud region is seen towards the north of the image. This boundary is now observed to be a real feature of the cloud field and not an artifact of the underlying sea ice boundary. An atmospheric correction was applied to the MAS spectral measurements using an above-cloud column water vapor amount of $0.95\ \mathrm{g\,cm^{-2}}$ (estimated from a SHEBA ice station rawinsonde launched at 2300 UTC for a cloud top height of 800 m). The correction follows the method of Platnick [1995]. Resulting optical thickness and effective radius retrievals using the 1.6 and 2.1 µm bands are shown in Figs. 6a,b. As expected, optical thickness retrievals do not show the underlying discontinuities observed in the visible band surface reflectance. In addition, effective radius retrievals are seen to be quite

uniform throughout the area, ranging from just 8-10 µm throughout much of the offshore cloud region. Figure 6c shows liquid water path derived from $LWP \approx 0.67 \tau r_e$, in units of $g m^{-2}$ with effective radius in micrometers. Though only exact for a vertically uniform cloud where differences between various relevant moments of the droplet size distribution can be ignored, the water path approximation is likely to be quite accurate (better than 10%) for similarly thick adiabatic clouds [*Platnick*, 2000]. Liquid water path results closely resemble the pattern of the optical thickness retrievals due to the small variability in effective radius across the region.

MAS retrieval statistics from the validation region (comprised of over 6,500 pixels) are given in Table 2a for the 1.6-2.1 µm band combination. The table also gives *in situ* profile measurements of the vertically integrated liquid water path and optical thickness (derived from the Gerber Scientific PVM-100A and cloud integrating nephelometer, respectively). Calibration coefficients for the PVM are traceable to standard methods [*Gerber et al.*, 1994] and recent glass bead tests. Accuracy of liquid water content measured with the PVM is estimated at ±5-10%. Nephelometer extinction measurements, at a visible wavelength, have an estimated uncertainty of ±10-15% [*Gerber et al.*, 2000]; the derived optical thickness uncertainty would be similar. The *in situ* effective radius consistent with the retrieval method is determined from a vertical weighting of the FSSP-100 measurements, assuming an adiabatic profile [*Platnick*, 2000]. The result is given in the table. Reasonable sub-adiabatic profiles (for example, a one-third reduction in upper cloud liquid water content) increase the expected retrieved radii by only several tenths of a micrometer. FSSP droplet effective radius measurements were found to be in excellent agreement with PVM-derived calculations (within a micrometer) when effective radii were 10 µm or less. The PVM effective radius measurements have an estimated uncertainty of ±10% for liquid water droplets based on 10 µm monodisperse glass bead tests, with an expected decrease in the PVM response for effective radii greater than 12-13 µm (not relevant to the clouds of this study). In summary, uncertainties for all *in situ* measurements given in the table are expected to be within about 10%.

Retrievals show a 20% overestimate in optical thickness relative to the *in situ* value, although effective radii agree to within a few percent. Liquid water path values are found to be in excellent agreement, although a water path estimate using the *in situ* optical thickness and effective radius (see above formula) is 13% lower than the integrated PVM measurements. This lack of consistency might be due, in part, to the use of an independent measurement source for each parameter, coupled with small-scale

microphysical variability. For instance, measured droplet effective radii at the same cloud level often varied by one to two micrometers on this day. Validation conclusions are also made difficult by the small *in situ* sample region (consisting of a single profile), compared with area-averaged reflectance retrievals (where reflected photons sample a horizontal region on the order of several hundred meters for the cloud in question). Given these caveats, the results of Table 2a are very encouraging.

When retrievals from the validation region were performed using the 1.6 and 3.7 μm MAS band combination, average effective radii were 14.0 μm (4-5 μm larger than when using the 2.1 μm band). Though some size discrepancy is expected since the average penetration depth varies with band droplet absorption, this large difference cannot be explained by the observed droplet size profile. Due to the lack of orthogonality seen in Fig. 2b, optical thickness retrievals were also larger by a similar fraction (average value of 15.3).

4.2 Mid-level stratus deck on June 3, 1998

A supercooled, mid-level stratus cloud (cloud-top temperature and height of 256 K and 3.3 km) covered the region of the SHEBA ice station on June 3, 1998. *In situ* profile measurements through the 600 m thick cloud layer were obtained just northeast of the ice station at 2122 UTC. Cloud integrating nephelometer analysis of the volume-averaged particle asymmetry parameter in the visible is consistent with the existence of spherical (liquid) cloud particles. Though several modes of ice crystals were observed by the University of Washington PMS 2D-C probe (maximum dimensions of about 200 μm and 2 mm), concentrations were very small, about 0.15 per liter, suggesting that the cloud layer was almost entirely liquid water. Lidar data from the SHEBA site also indicates liquid water droplets at the overpass times (*T. Uttal and B. Orr*, personal communication). Measurement statistics are summarized in Table 2b. The upper range given for optical thickness accounts for the presence of a lower, separate cloud layer, observed between an altitude of 0.5-1 km during the Convair-580 profile. This lower layer is found to contribute an additional optical path of only 3, compared with about 11 for the mid-level cloud layer. Over the SHEBA site, radar and lidar data indicate the dissipation of a thin lower layer at about 2200 UTC. However, the large-scale persistence of this optically thin layer throughout the validation region is not certain. Regardless, the potential ice particle contribution to optical extinction from either layer is likely to be insignificant, and so a liquid water retrieval algorithm should be suitable for the combined layers, if present.

The ER-2 flew over the same cloud region at 2103 UTC (about 20 minutes before the Conviar-580 sampling). A MAS visible image of this region is shown in the left panel of Fig. 7a (not geolocated); the imaged area is approximately 37 km in the east-west dimension by 31 km north-south. The *in situ* measurements are well north of the distinct east-west cloud band whose northern boundary is seen just to the south of the ice station (note the eddies seen throughout the northern boundary region, apparently caused by horizontal shear-induced turbulence). A subsequent ER-2 overpass towards the southeast was made over the ice station about 30 minutes later (10 minutes after the *in situ* profile) allowing two flight tracks to be included in the validation. The second pass showed the cloud band to be advecting to the north-northwest at about 4.5 ms^{-1}. The shape of the northern edge of the boundary was preserved during this time. It will be shown (Fig. 7a) that retrieval differences across this boundary can be significant, especially for effective radius. Variability within each cloud region is also substantial. It is therefore important to co-locate the cloud region corresponding to the Convair-580 measurements with MAS imagery from the two ER-2 overpasses at earlier and later times.

Assuming that all cloud parcels move with the same mean flow as the boundary, a simple estimate can be made for the forward and backward trajectory of the sampled cloud. In this manner, optical thickness and effective radius retrievals were averaged from the two flight tracks (an unweighted average of over 17,000 pixels from the first overpass image, and 4,000 pixels from the second overpass). An atmospheric correction was based on an above-cloud column water vapor amount of 0.3 gcm^{-2} (derived from a SHEBA rawinsonde launched from the ice station at 2300 UTC). Results, shown in Table 2b for the 1.6 and 2.1 μm band retrievals, are again in good agreement with the airborne *in situ* measurements. In contrast to the results of section 4.1, the *in situ* estimate of liquid water path based on optical thickness and effective radius agrees well with the retrievals, but is in excess of the integrated liquid water content measurement. The large-scale retrievals are shown in Fig. 7a. Liquid water path (not shown) ranges from about 30 gm^{-2} in the southern region as well as just to the north of the cloud band in the western edge of the image, to a maximum of about 110 gm^{-2} in the eastern eddies just inside the cloud band.

For comparison, retrievals made with the 1.6 and 3.7 μm bands are shown in Fig. 7b. Effective radius retrievals are larger by about 3 μm (an average of 11.2 μm) with a corresponding optical thickness increase of 55%. The cause of this large retrieved effective radius discrepancy for both cloud case studies is unknown. MAS retrievals of

summertime California marine stratocumulus clouds have also shown significantly larger effective radii when using the 3.7 µm and nonabsorbing band combination [*Platnick et al.*, 2000]. In fact, absolute size retrieval differences are generally the same, about 4-5 µm. As already mentioned, measured droplet size profiles do not account for the difference. For comparison, a retrieval case study for marine stratocumulus using the Advanced Very High Resolution Radiometer (AVHRR) 3.7 µm channel on the NOAA polar orbiting satellites yielded better droplet size agreement [*Platnick and Valero,* 1995]. MAS radiometric measurements in the 3.7 µm band would have to be increased by about 20% to give retrievals consistent with *in situ* profile measurements and 2.1 µm band retrievals. Though instrument calibration is always a potential issue, emissivity analysis of the onboard blackbodies used in processing the 3.7 µm band data is not thought to be a source for such an error. Increasing the amount of above-cloud water vapor absorption acts to reduce retrieved radii. However, for the June 3 case study, an increase in the column amount by over a factor of 9 (reduction in the 3.7 µm band above-cloud nadir transmittance from 0.95 to 0.83) would be required to move retrievals into the *in situ* range. It should be noted that top-of-the-atmosphere solar spectral fluxes used in computing cloud reflectance for this band are in need of modern corroboration. A common source of data is from the compilation of *Thekaekara* [1974], which reports fluxes at 100 nm intervals through this band. The 3.7 µm band retrieval issue is clearly in need of further study.

5. Discussion and conclusions

An algorithm for retrieving cloud optical thickness and droplet effective radius over snow and ice surfaces has been developed. Retrievals have been applied to imagery obtained from the MODIS Airborne Simulator (MAS) instrument flown aboard the high altitude NASA ER-2 during the Arctic FIRE-ACE field deployment from May-June 1998. Results from two case studies have been compared with *in situ* measurements from the University of Washington Convair-580 aircraft.

The retrieval technique uses only a combination of spectral bands for which the snow/ice surface albedo is relatively small, and eliminates the use of visible and other bands for which the surface reflectance is large. A large surface reflectance is problematic for two reasons. First, as demonstrated in section 2, it is not likely that the surface reflectance can be specified to the level of accuracy needed for useful optical thickness retrievals. This applies to the spatial and temporal scales needed for global

studies, as well as small-scale validation exercises near coastal or other transitional areas. Secondly, even if the surface reflectance is specified accurately, a large value diminishes the impact of the cloud contribution to the overall reflectance. This effectively reduces the sensitivity of aircraft or satellite measurements to cloud optical thickness, or conversely, the optical thickness retrieval error is increased for the same amount of measurement or cloud modeling error. However, a 1.6 μm band reflectance measurement, combined with a 2.1 μm or 3.7 μm band measurement, has sufficient information content for performing retrievals. In a sense, the 1.6 μm band is used as a surrogate for the traditional band (e.g., 0.67, 0.86 μm bands) where insignificant water droplet absorption provides a nearly independent estimate of cloud optical thickness. The advantage in this modified algorithm is that each of these longer wavelength bands has a small snow/ice surface reflectance during the time frame of the FIRE-ACE experiment (similar to dark open water). Earlier in the springtime (April), spectral sea ice albedo derived from the CAR instrument is significantly larger than in June for all bands, including the 1.6 μm band, due to snow cover on the sea ice (see Fig. 3). For such a situation, algorithm advantages may not be as significant. The disadvantage with this technique is that the two cloud parameters are no longer orthogonal through much of the measurement space due to droplet absorption in the 1.6 μm band. An increased sensitivity to measurement error may exist compared with traditional retrievals over dark surfaces.

MAS retrievals were made for several liquid water clouds during FIRE-ACE, including the two extensive stratus case studies discussed here: a low boundary layer cloud and a mid-level supercooled cloud. In both cases, retrievals are in close agreement with Convair-580 *in situ* measurements when the 1.6–2.1 μm MAS band combination is used. However, when using the 3.7 μm band, effective radius retrievals are found to be 3-5 μm larger than expected from cloud profile measurements. The source of this discrepancy is not clear. An overall impression is that results for the FIRE-ACE clouds appear very similar to previous retrievals on warm marine boundary layer stratocumulus. Future efforts will use the algorithm to derive retrieval statistics from all useful liquid water cloud observations during the ER-2 deployment period. The initial success of the technique has important implications for the future development of robust operational satellite cloud retrieval algorithms in polar and wintertime regions.

Acknowledgments. This work was supported in part by funding provided by the NASA Radiation Science Program, the MODIS Science Team, and the EOS Project Science Office. The authors wish to thank G. T. Arnold at NASA Goddard Space Flight Center; A. Rangno at the University of Washington; T. Uttal, J. Intrieri, and B. Orr of NOAA/ETL; M. Fitzgerald, P. Hajek, and J. Myers at the NASA Ames Research Center and C. Moeller at the University of Wisconsin for MAS processing and calibration support. Ice station rawinsonde data were obtained from the SHEBA web site courtesy of the University of Washington Applied Physics Laboratory.

References

Albrecht, B.A., Aerosols, cloud microphysics, and fractional cloudiness, *Science*, *245*, 1227-1230, 1989.

Arking, A., and J.D. Childs, Retrieval of cloud cover parameters from multispectral satellite images, *J. Climate Appl. Meteor.*, *24*, 322-333, 1985.

Arnold, G.T., S.C. Tsay, M.D. King, J.Y. Li, and P.F. Soulen, Airborne spectral measurements of surface-atmosphere anisotropy for Arctic sea ice and tundra, *Int. J. Remote Sens.* (submitted), 2000.

Austin, P., Y. Wang, R. Pincus, and V. Kujala, Precipitation in stratocumulus clouds: observational and modeling results, *J. Atmos. Sci.*, *52*, 2329-2352, 1995.

Bohren, C.F., Multiple scattering of light and some of its observable consequences, *Amer. J. Phys.*, *55*, 524-533, 1987.

Charlson, R.J., J.E. Lovelock, M.O. Andreae, and S.G. Warren, Oceanic phytoplankton, atmospheric sulphur, cloud albedo and climate, *Nature*, *326*, 655-661, 1987.

Curry, J.A., et al., FIRE Arctic Clouds Experiment, *Bull. Amer. Meteor. Soc.*, 81, 5-30, 2000.

DeAbreu, R.A., D.G. Barber, K. Misurak, and E.F. LeDrew, Spectral albedo of snow-covered first-year and multi-year sea ice during spring melt, *Ann. Glaciol.*, *21*, 337-342, 1995.

Foot, J.S., Some observations of the optical properties of cloud. Part I: Stratocumulus, *Quart. J. Roy. Meteor. Soc.*, *114*, 129-144, 1988.

Gerber, H., B.G. Arends, and A.S. Ackerman, New microphysics sensor for aircraft use, *Atmos. Res.*, *31*, 235-252, 1994.

Gerber, H., Y. Takano, T. J. Garrett, and P. V. Hobbs, Nephelometer measurements of the asymmetry parameter, volume extinction coefficient and backscatter ratio in Arctic clouds, *J. Atmos. Sci.*, (in press), 2000.

Grenfell, T.C., and D.K. Perovich, Spectral albedo of sea ice and incident solar irradiance in the southern Beaufort Sea, *J. Geophys. Res.*, *89*, 3573-3580, 1984.

Han, Q., W.B. Rossow, and A.A. Lacis, Near-global survey of effective droplet radii in liquid water clouds using ISCCP data, *J. Climate*, *7*, 465-497, 1994.

King, M. D., M. G. Strange, P. Leone, and L. R. Blaine, Multiwavelength scanning radiometer for airborne measurements of scattered radiation within clouds, *J. Atmos. Oceanic Tech.*, *3*, 513-522, 1986.

King, M.D., W.P. Menzel, P.S. Grant, J.S. Myers, G.T. Arnold, S.E. Platnick, L.E. Gumley, S.C. Tsay, C.C. Moeller, M. Fitzgerald, K.S. Brown, and F.G. Osterwisch, Airborne scanning spectrometer for remote sensing of cloud, aerosol, water vapor, and surface properties, *J. Atmos. Oceanic Tech.*, *13*, 777-794, 1996.

Kratz, D. P., The correlated k-distribution technique as applied to AVHRR channels, *J. Atmos. Sci.*, *51*, 1823-1842.

Nakajima, T., and M.D. King, Determination of the optical thickness and effective particle radius of clouds from reflected solar radiation measurements. Part I: Theory, *J. Atmos. Sci.*, *47*, 1878-1893, 1990.

Nakajima, T., M.D. King, J.D. Spinhirne, and L.F. Radke, Determination of the optical thickness and effective particle radius of clouds from reflected solar radiation measurements. Part II: Marine stratocumulus observations, *J. Atmos. Sci.*, *48*, 728-750, 1991.

Ou, S.C., K.N. Liou, Y. Takano, N.X. Rao, Q. Fu, A.J. Heymsfield, L.M. Miloshevich, B. Baum, and S.A. Kinne, Remote sounding of cirrus cloud optical depths and ice crystal sizes from AVHRR data: Verification using FIRE II IFO measurements, *J. Atmos. Sci.*, *52*, 4143-4158, 1995.

Pincus, R., and M.B. Baker, Effect of precipitation on the albedo susceptibility of clouds in the marine boundary layer, *Nature*, *372*, 250-252, 1994.

Platnick, S., Vertical photon transport in cloud remote sensing problems, *J. Geophys. Res.*, (submitted), 2000.

Platnick, S., P.A. Durkee, K. Nielsen, J.P. Taylor, S. C. Tsay, M.D. King, R.J. Ferek, P.V. Hobbs, and J.W. Rottman, The role of background cloud microphysics in the radiative formation of ship tracks, *J. Atmos. Sci.*, (in press), 2000.

Platnick, S., and S. Twomey, Determining the susceptibility of cloud albedo to changes in droplet concentrations with the Advanced Very High Resolution Radiometer, *J. Appl. Meteor.*, *33*, 334-347, 1994.

Platnick, S., and F.P.J. Valero, A validation of a satellite cloud retrieval during ASTEX, *J. Atmos. Sci.*, *52*, 2985-3001, 1995.

Perovich, D. K., Light reflection from sea ice during the onset of melt, *J. Geophys. Res.*, *99*, 3351-3359, 1994.

Rawlins, F., and J.S. Foot, Remotely sensed measurements of stratocumulus properties during FIRE using the C130 aircraft multi-channel radiometer, *J. Atmos. Sci.*, *47*, 2488-2503, 1990.

Rolland, P., K. N. Liou, M. D. King, S. C. Tsay, and G. M. McFarquhar, Remote sensing of optical and microphysical properties of cirrus clouds using MODIS channels: Methodology and sensitivity to assumptions, *J. Geophys. Res.*, (in press), 2000.

Salisbury, J. W., D. M. D'Aria, and A. Wald, Measurements of thermal infrared spectral reflectance of frost, snow, and ice, *J. Geophys. Res.*, *99*, 24235-24240, 1994.

Slingo, A., Sensitivity of the Earth's radiation budget to changes in low clouds, *Nature*, *343*, 49-51, 1990.

Soulen, P. F., M. D. King, S. C. Tsay, G. T. Arnold, and J. Y. Li, Airborne spectral measurements of surface-atmosphere anisotropy during SCAR-A, Kuwait oil fire, and TARFOX experiments, *J. Geophys. Res.*, *105*, 10203-10218, 2000.

Thekaekara, M.P., Extraterrestrial solar spectrum, 3000-6100 Å at 1-Å intervals, *Appl. Opt.*, *13*, 518-522, 1974.

Tsay, S.C., M.D. King, G.T. Arnold, and J.Y. Li, Airborne spectral surface measurements of surface anisotropy during SCAR-B, *J. Geophy. Res.*, *103*, 31943-31953, 1998.

Twomey, S., Pollution and the planetary albedo, *Atmos. Environ.*, *8*, 1251-1256, 1974.

Twomey, S., Aerosols, clouds, and radiation, *Atmos. Environ.*, *25A*, 2435-2442, 1991.

Twomey, S., and T. Cocks, Spectral reflectance of clouds in the near-infrared: Comparison of measurements and calculations, *J. Meteor. Soc. Japan*, *60*, 583-592, 1982.

Twomey, S., and T. Cocks, Remote sensing of cloud parameters from spectral reflectance in the near-infrared, *Beitr. Phys. Atmos.*, *62*, 172-179, 1989.

Warren, S. G., Optical constants of ice from the ultrviolet to the microwave, *Appl. Opt.*, *23*, 1206-1225, 1984.

Wielicki, B.A., R.D. Cess, M.D. King, D.A. Randall, and E.F. Harrison, Mission to Planet Earth - role of clouds and radiation in climate, *Bull. Amer. Meteor. Soc.*, *76*, 2125-2153, 1995.

Young, D.F., P. Minnis, D. Baumgardner, and H. Gerber, Comparison of in situ and satellite-derived cloud properties during SUCCESS, *Geophys. Res. Lett.*, *25*, 1125-1128, 1998.

List of Figures

Fig. 7a. MAS visible band image (far left) showing a mid-level liquid water stratus deck (cloud top heights at approximately 3.3 km throughout the three distinct cloud regions) on June 3, 1998 in the vicinity of the SHEBA ice station. Corresponding retrievals using the 1.6 and 2.1 μm MAS bands are shown to the right. The approximate location of the cloud region sampled by the *in situ* probes about 10 minutes after the overpass is also indicated. The imaged area is 37 km in the east-west direction by 31 km in the north-south.

Fig. 7b. Same as in Fig. 7a, but for retrievals using the 1.6 and 3.7 μm MAS bands.

Table 1. Sensitivity of retrievals to uncertainty in the measured reflectances R_1 and R_2 corresponding to two spectral bands λ_1 and λ_2. Calculated for a cloud with τ_c=10, r_e=10, and geometry given by μ=0.85, μ_0=0.55, and an azimuth average (same as Figs. 1,2).

Sensitivity	**Retrieval band combinations (λ_1, λ_2 in μm):**					
	0.67[a], 2.1	0.67 [a], 3.7	0.67 [b], 2.1	0.67 [b], 3.7	1.6, 2.1	1.6, 3.7
$\frac{\partial \ln \tau_c}{\partial \ln R_1}$	2.4	2.2	5.8	5.6	3.8	2.9
$\frac{\partial \ln \tau_c}{\partial \ln R_2}$	-0.5	-0.2	-0.2	-0.1	-1.7	-0.6
$\frac{\partial \ln r_e}{\partial \ln R_1}$	0.8	0.01	1.9	0.04	1.2	0.02
$\frac{\partial \ln r_e}{\partial \ln R_2}$	-1.9	-0.8	-1.8	-0.8	-2.2	-0.8

[a] *Calculated with a surface albedo of 0.06 for the 0.67 μm band*; [b] *surface albedo of 0.50 for the 0.67 μm band. Near-infrared surface albedos are 0.04.*

Table 2a. MAS retrieval summary compared with University of Washington Convair-580 *in situ* measurements, for a boundary layer stratocumulus cloud on June 6, 1998.

Parameter	MAS retrievals* (statistics)	UW Convair-580 (derived from profile measurements)
τ	10.4	8.6 [1]
σ_τ	1.7	
r_e (μm)	9.3	9.0 [2]
σ_{re}	1.1	
LWP (g m^{-2})	64	60 [3]
σ_{LWP}	10	

Table 2b. MAS retrieval summary (derived from two flight tracks) compared with University of Washington Convair-580 *in situ* measurements, for a mid-level liquid water stratus deck on June 3, 1998.

Parameter	MAS retrievals* (statistics)	UW Conviar-580 (derived from profile measurements)
τ	14.4	10.7-13.9 [1]
σ_τ	1.5	
r_e (μm)	8.3	8.1 [2]
σ_{re}	0.6	
LWP (g m^{-2})	80	45-56 [3]
σ_{LWP}	10	

** retrievals using 1.6 μm and 2.1 μm MAS bands; [1] Cloud Integrating nephelometer, Gerber Scientific, Inc.; [2] FSSP-100 (expected retrieval range based on adiabatic vertical profile); [3] PVM-100A.*

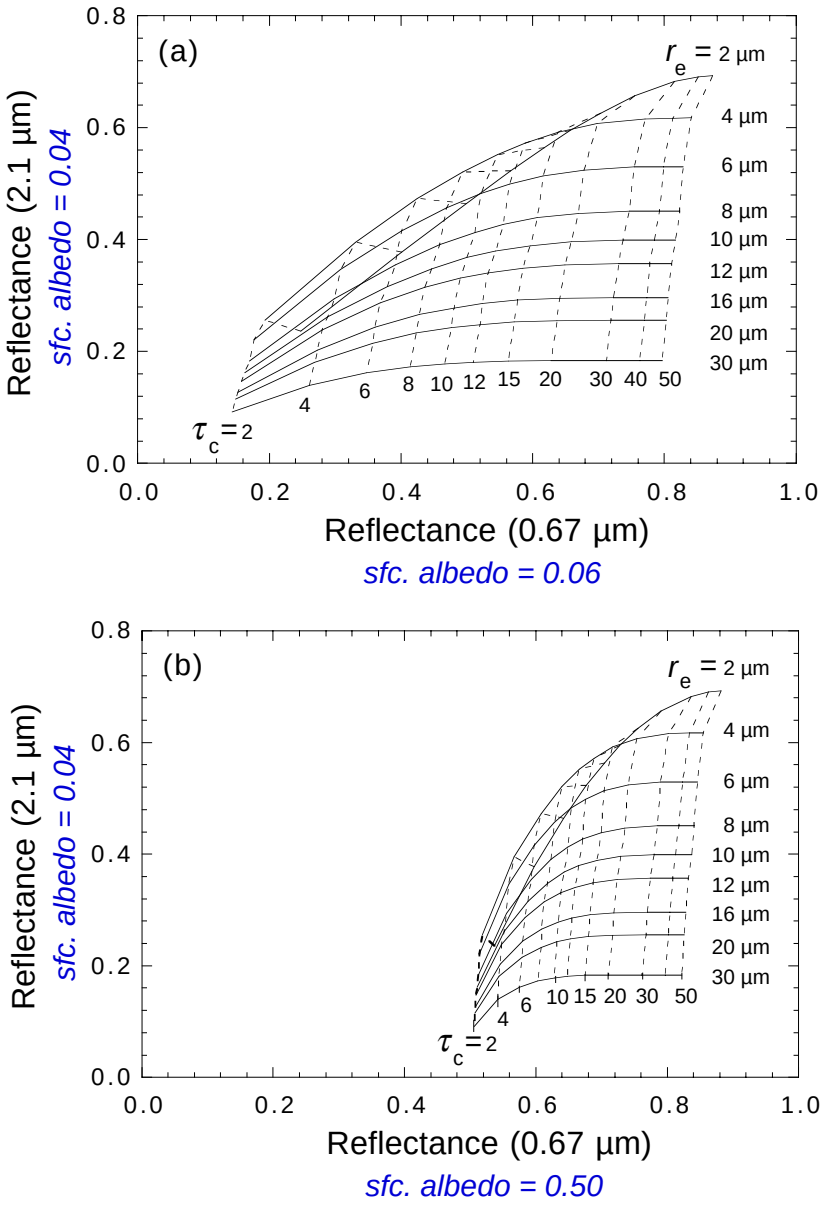

Figure 1. Cloud retrieval solution space showing contours of constant optical thickness (τ_c - dashed lines) and droplet effective radius (r_e - solid lines) as a function of 0.67 and 2.1 µm band reflectances. A point specified by measurements in the two spectral bands gives the solution. Two different surface albedos in the visible are considered: (a) Lambertian reflectance of 0.06 corresponding to open water, and (b) reflectance of 0.50 corresponding to sea ice. Calculations are for $\mu_0 = 0.55$, $\mu = 0.85$, and an azimuthal average.

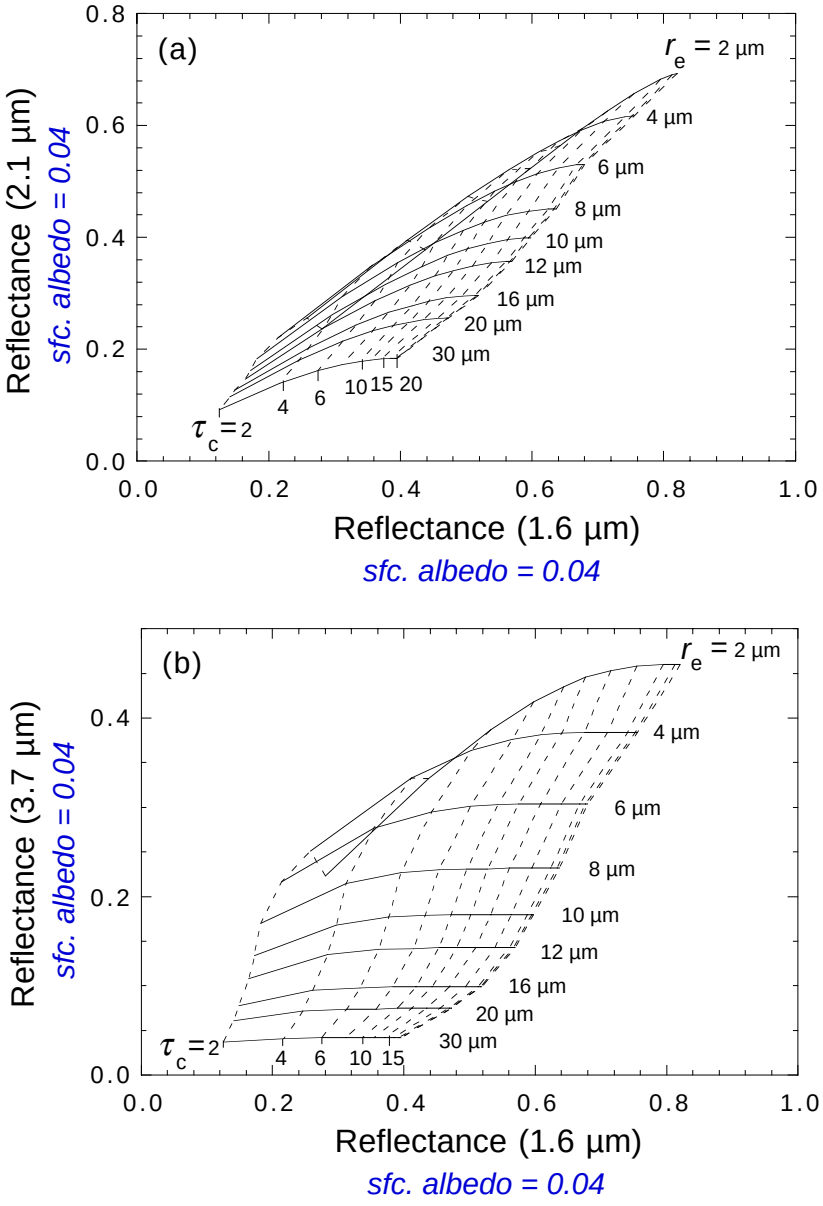

Figure 2. Same as Fig. 1, but retrieval solution space as a function of (a) 1.6 and 2.1 µm band reflectances, and (b) 1.6 and 3.7 µm band reflectances. Surface albedos in both spectral bands are consistent with the Arctic snow/ice measurements described in the text.

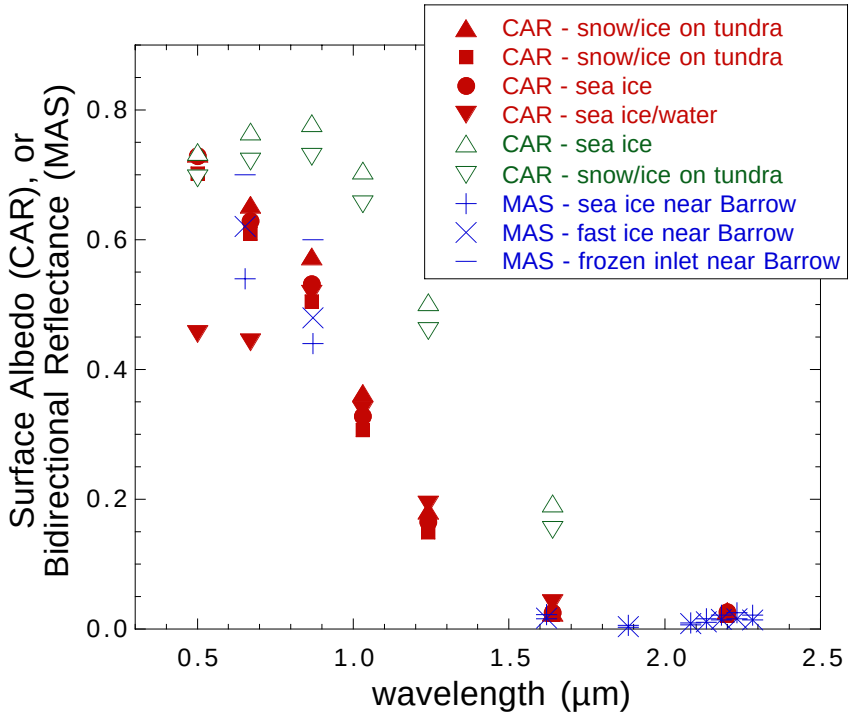

Figure 3. Sea ice and snow albedo derived from CAR measurements in the vicinity of Prudhoe Bay, Alaska during April 1992 (LEADEX, open triangles) and June 1995 (ARMCAS, closed symbols). Also shown are selected MAS sea ice bidirectional reflectance measurements on May 29, 1998 during FIRE-ACE.

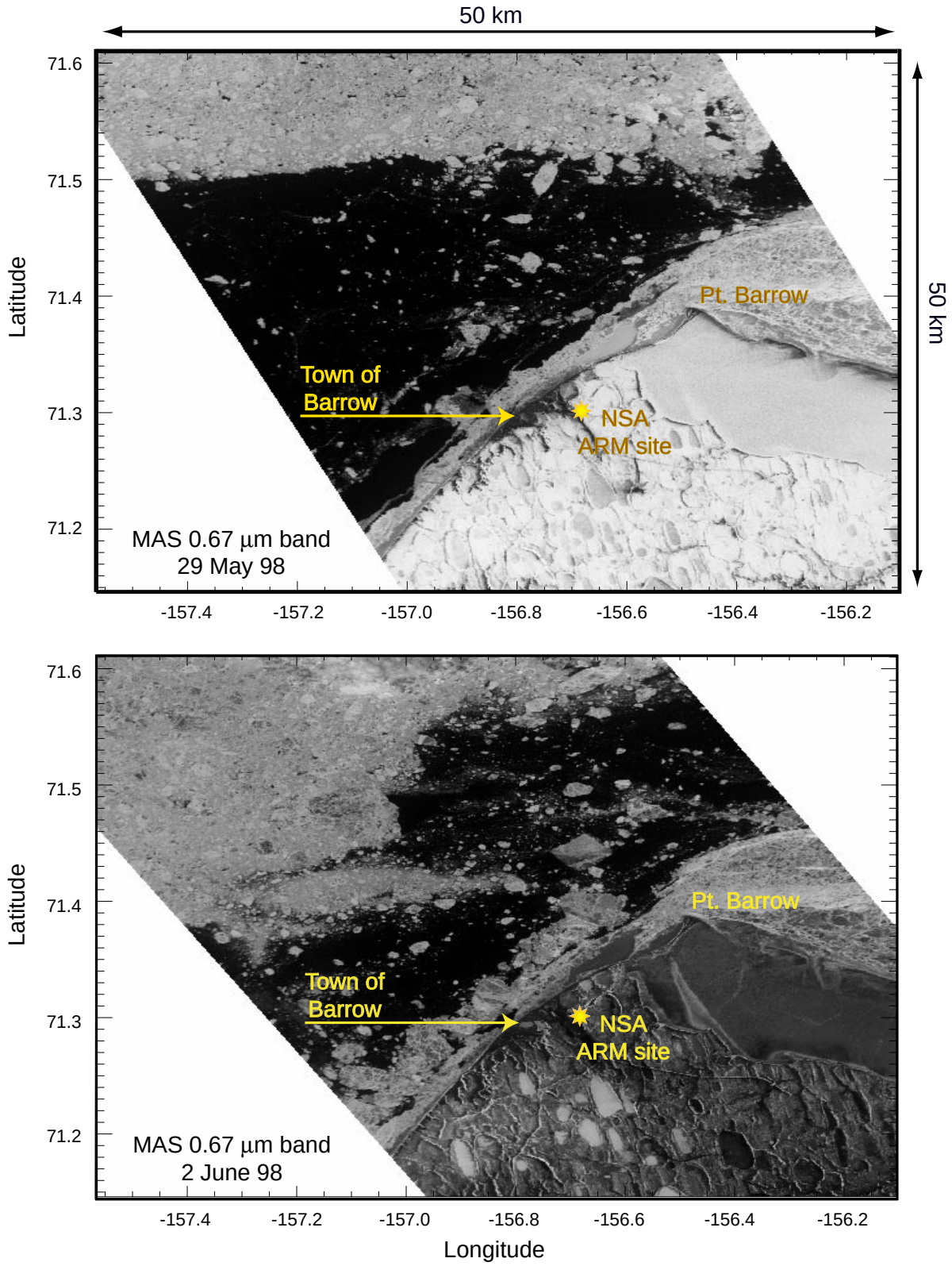

Figure 4. MAS 0.67 µm band geolocated images of the Barrow, Alaska area on two clear-sky days: May 29, 1998 (top image) and June 2, 1998 (bottom). Complete melting of snow on the tundra occurred during the four days between images, along with significant movement of offshore ice.

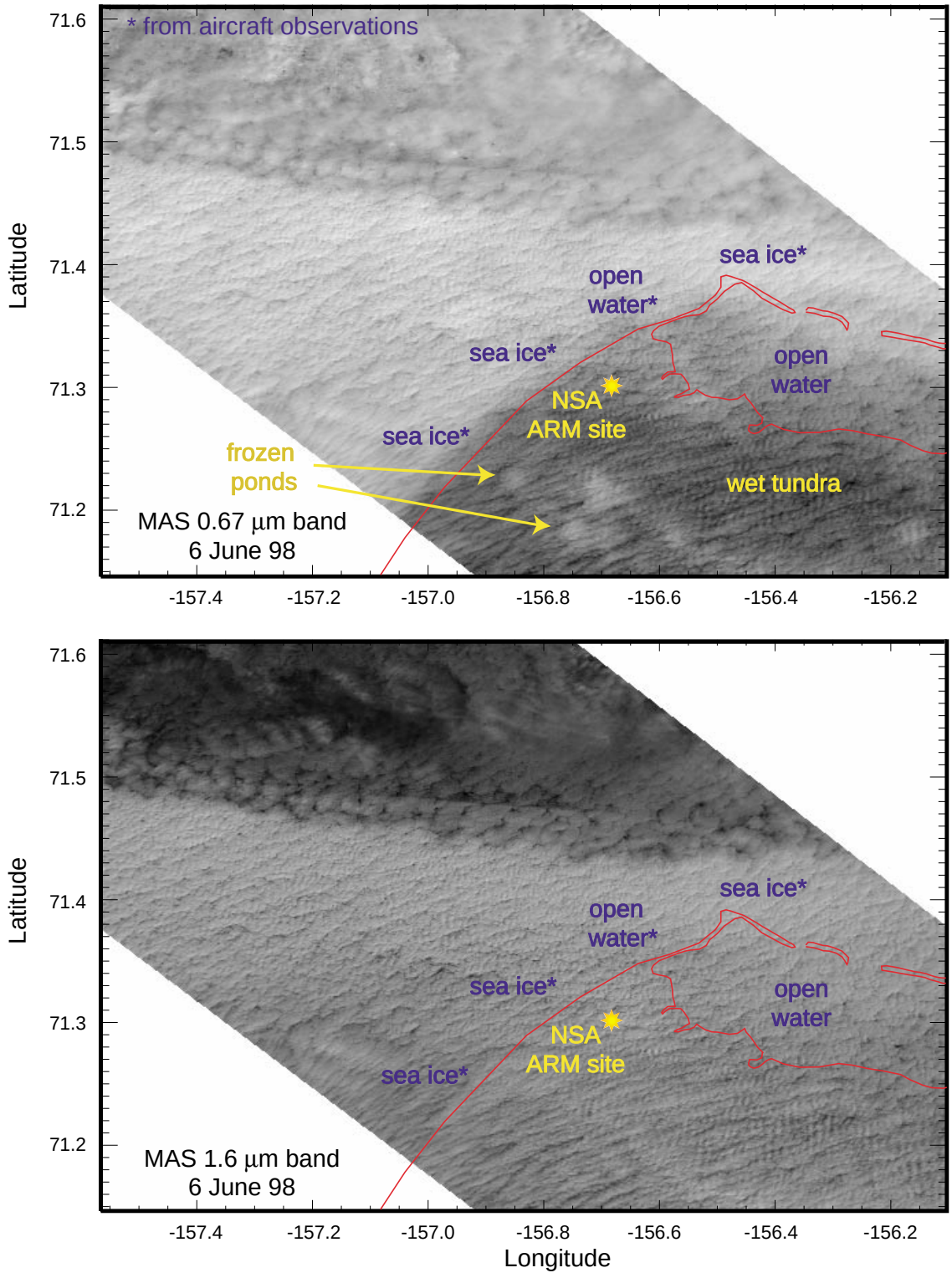

Figure 5. MAS 0.67 µm band geolocated image of an extensive low-level stratus deck in the Barrow area on June 6, 1998 (top image) where differing surface reflectances are clearly seen through the cloud. Corresponding 1.6 µm image (bottom) with small surface reflectances for snow, ice, and wet tundra indicates a relatively uniform cloud across the land-ocean boundary.

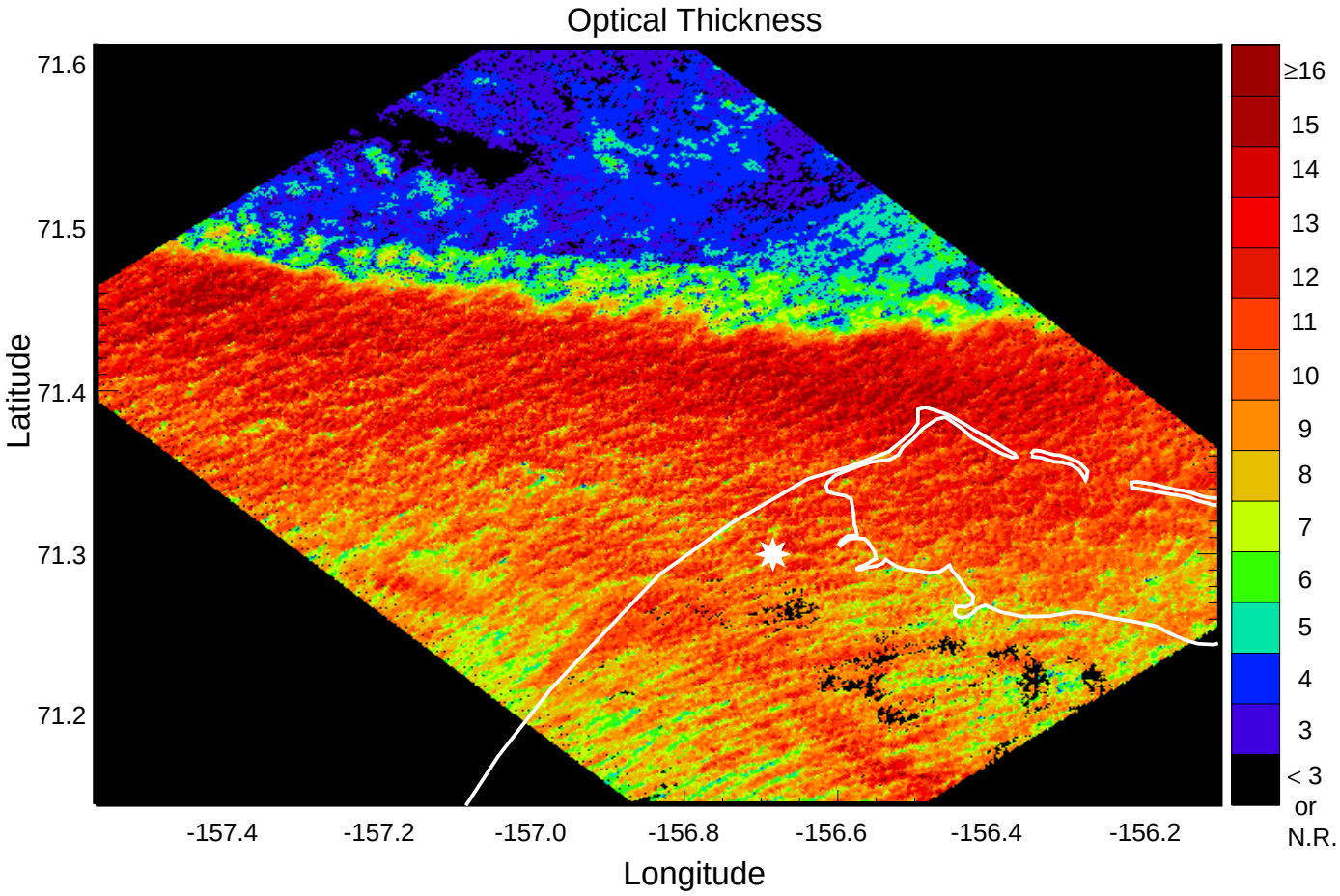

Figure 6a. Cloud optical thickness retrievals for the June 6, 1998 low-level stratus deck of Fig. 5 using MAS 1.6 and 2.1 μm bands. Optical thickness is seen to be continuous across the land-ocean boundary while a dramatic decrease is seen across the cloud boundary to the north. The notation *N.R.* on the color bar refers to no retrieval.

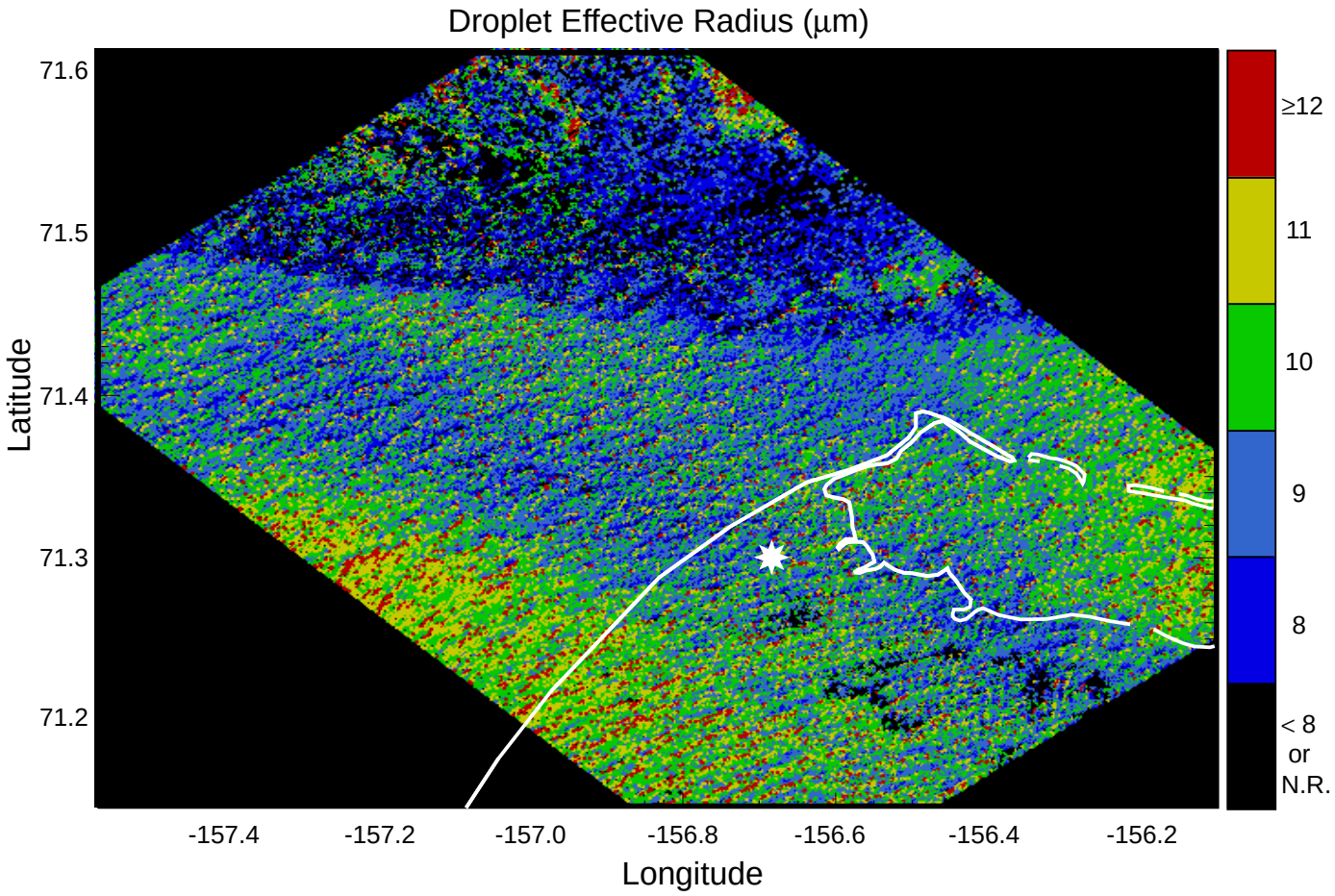

Figure 6b. Same as in Fig. 6a, but retrieval of cloud droplet effective radius.

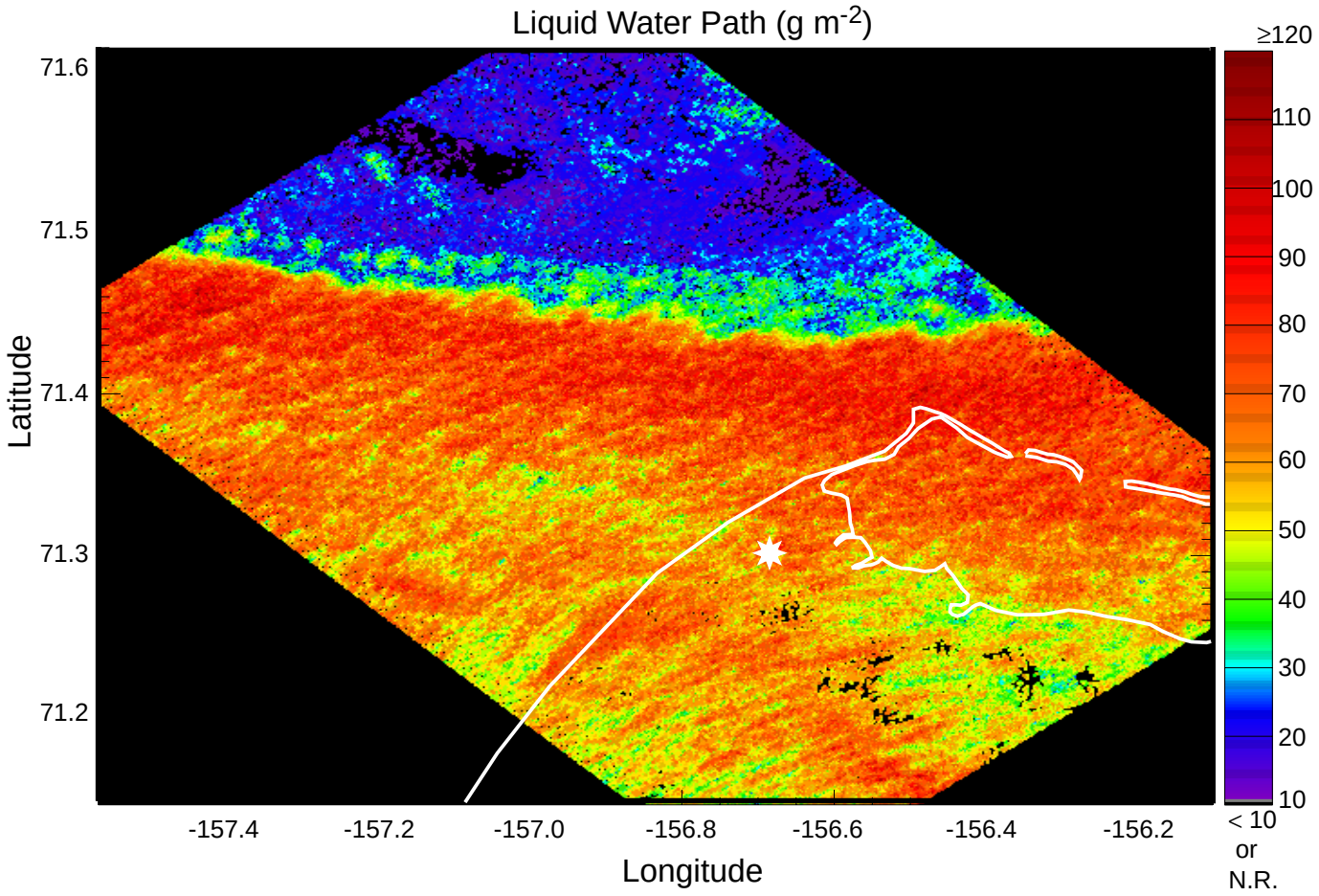

Figure 6c. Same as in Fig. 6a, but retrieval of cloud liquid water path.

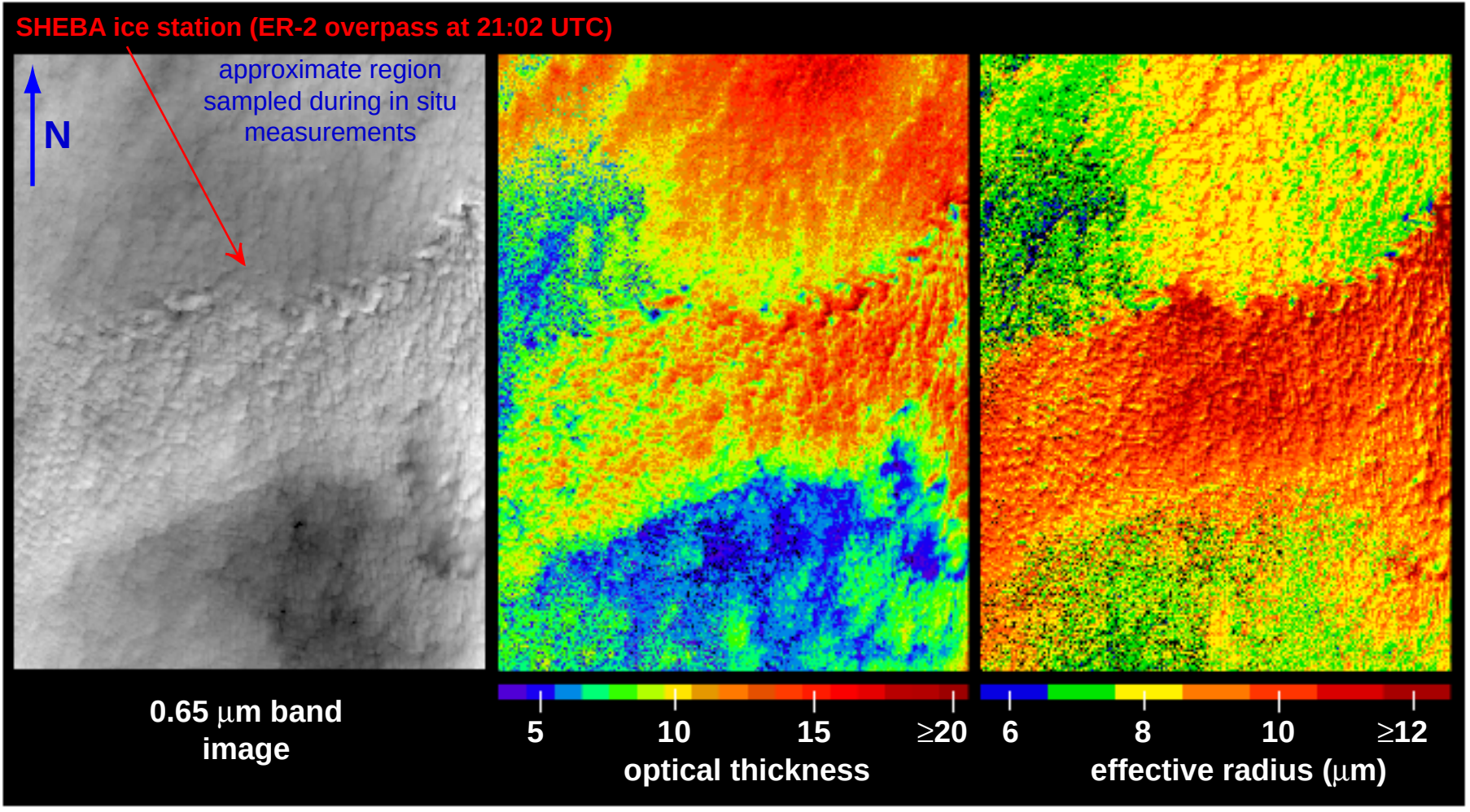

Figure 7a. MAS visible band image (far left) showing a mid level liquid water stratus deck (cloud top heights approximately 3.3 km throughout the three distinct cloud regions) on June 3, 1998 in the vicinity of the SHEBA ice station. Corresponding retrievals using the 1.6 and 2.1 μm MAS bands are shown to the right. The approximate location of the cloud region sampled by the *in situ* probes about 10 minutes after the overpass is also indicated. The imaged area is 37km in the east-west direction by 31km in the north-south.

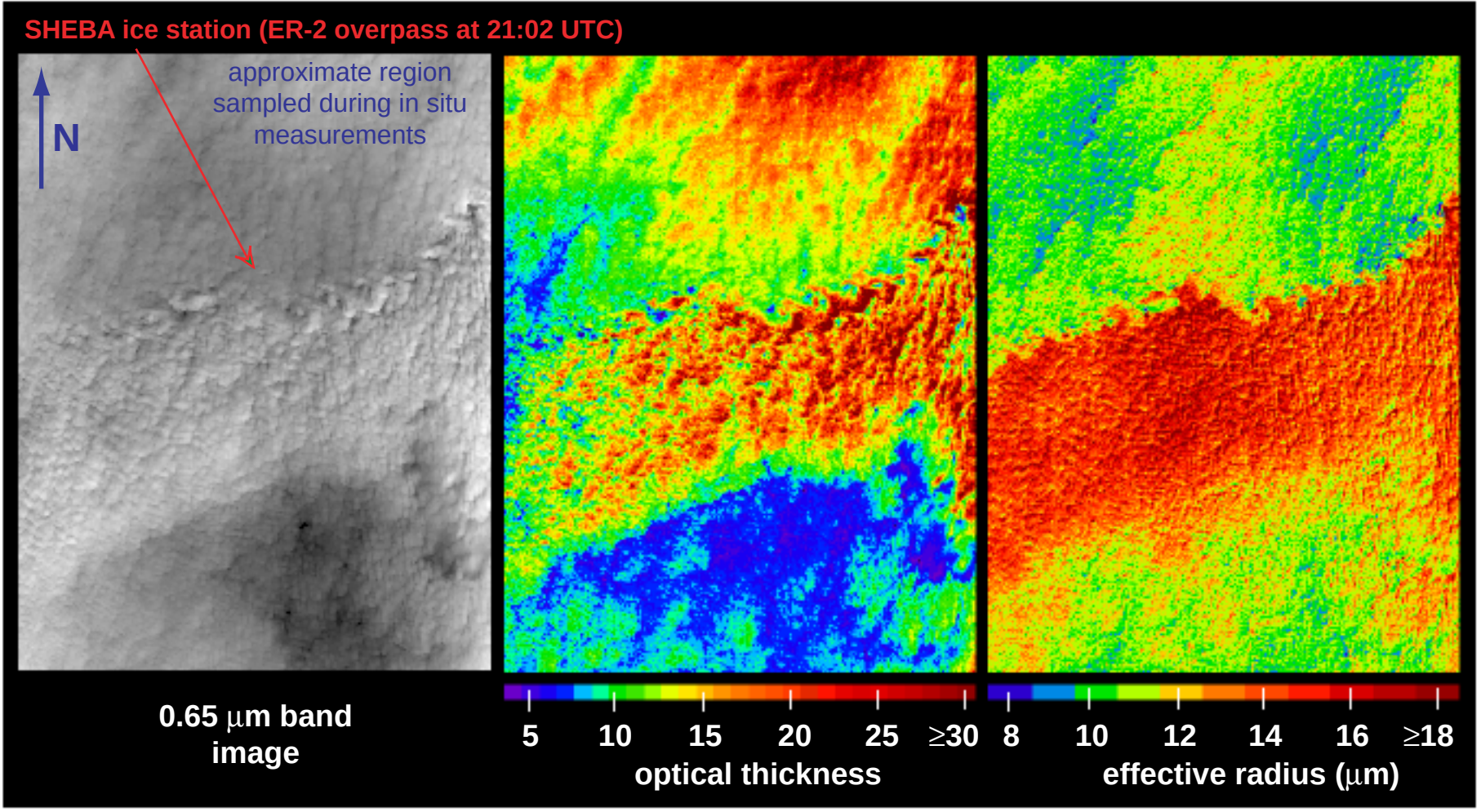

Figure 7b. Same as Fig. 7a, but for retrievals using the 1.6 and 3.7 μm MAS bands.